Geometric Calibration for Offset Flat-panel CBCT Systems using Projection Matrix

Van-Giang Nguyen
Department of Information Systems
Le Quy Don Technical University, Hanoi, Vietnam
giangnv@mta.edu.vn

***Abstract*— Geometric parameters that define the system geometry are crucial for image reconstruction in X-ray computed tomography (CT). This paper considers the problem of determining geometric parameters for an offset flat-panel cone beam CT (CBCT) system, a recently introduced modality with a large field of view, with assumption of unstable mechanism. To find the geometric parameters for each projection view, we use projection matrix method and design a dedicated phantom that is partially visible in all projection views. The phantom consists of balls distributed symmetrically in a cylinder to ensure the use of phantom in all views. To compensate for imperfect placement of balls in phantom and the non-symmetry of ball shapes, and to prevent the errors in estimated geometric parameters when using in reconstruction, instead of decomposing the projection matrix into actual geometric parameters which are then manually corrected before using in reconstruction, we directly use the projection matrix and its pseudo inverse for projection and backprojection in reconstruction. The experiments illustrate the efficacy of the proposed method with a real offset flat-panel CBCT system in dental imaging.**

Keywords—Geometric calibration, image reconstruction, perspective geometry, inverse problems, computed tomography

I. INTRODUCTION

X-ray computed tomography (CT) is an imaging technique that provides anatomical information about the object and is now a major imaging modality in medicine. In CT imaging, the images showed to the doctor are not directly acquired from scanner but reconstructed from projection data [1].

One major requirement in all reconstruction algorithms in CT imaging is the knowledge about the geometry of imaging system (CT scanner). Minor errors in geometric parameters result in major artefacts in reconstruction [2]. In ideal condition, one can assume that the system is perfectly manufactured and the geometric parameters are highly accurate before shifting to the practical usages. However, due to the unwanted factors when shifting the scanner, the degradation of the system from time and human factors, the pre-calculated geometric parameters are less reliable. Those facts lead to the requirement of a method to automatically measure geometric parameters of the X-ray scanner.

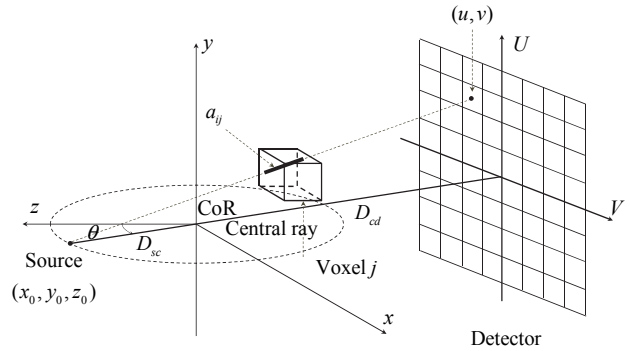

Fig. 1. Cone-beam CT geometry and its 3D to 2D projection.

Existing geometric calibration methods can be classified into two categories: phantom-based (offline) methods [3]-[5] and phantom-less (online) methods [6]-[9]. In phantom-based methods, the projection of a calibration phantom (which consists of several ball-shape markers) is first carried and followed by computation to estimate geometric parameters. The calibration process has three steps: (i) Measure the projected location of markers (and their center points) in the projection image; (ii) Setup equations that relate the founded locations in step (i) and the pre-defined position of markers in the phantom; (iii) Solve the equation to find geometric parameters. Despite its difficulties in designing phantom, phantom-based methods achieves highly accurate results [5]. In phantom-less methods, the geometric parameters are calculated directly from the projection images without the use of a calibration phantom. The computation relies on complex optimization whose objective functions are in projection domain [6] or in reconstructed volume domain [9]-[11]. (See [8] for more information). However, these methods suffer expensive computation load as well as unstable results.

Regarding its abilities, geometric calibration methods can be classified into view-independent and view-dependent methods. The first ones assume a stable mechanism and are met in high-end CT systems. Meanwhile, the later ones are

This research is funded by Vietnam National Foundation for Science and Technology Development (NAFOSTED) under grant number 102.01-2013.42.

usually met in practice. This is due to the imperfect of the scanner, the imbalance of the suspension arm holding X-ray source and detector, as well as the non-symmetry of the scanner, especially in mid- and low-end ones with flat-panel detector. Among many methods to estimate geometric parameters for each view, the projection matrix-based method is the most widely used one, especially in clinical practice and industry, due to its fast computation and reliable results. It has been shown to provide state-of-the-art result (in comparison with other existing methods).

Offset flat-panel CBCT systems are recently introduced CBCT systems with applications in multimodality systems (such as PET/CT and SPECT/CT) and dental imaging. However, due to its imbalance mechanism, geometric calibration for it is difficult and yet to be thoroughly considered. In this work, we develop a projection matrix-based method for calibrating offset flat-panel CBCT. The new method comes with a dedicated phantom for offset flat-panel CT systems as well as a new technique to prevent numerical errors which are usually involved in conventional projection matrix method. In particular, instead of decomposing the projection matrix into subsequent geometric elements which are then manually corrected, we directly use the projection matrix and its pseudo inverse matrix in reconstruction process. This technique is not only useful for offset flat panel CBCT systems, but also for other CBCT systems.

The remainder of this paper is organized as follows. Section II presents projection matrix-based calibration method, geometry and calibration phantom for offset flat-panel CBCT, the use of projection matrix in backprojection and projection of a representative reconstruction algorithm. Section III presents our experiment studies. Section IV discusses and concludes.

II. METHODS

A. Review of Projection matrix-based Calibration Method

In X-ray imaging, given a point source (X-ray source) and a two-dimension (2D) detector, a point (x, y, z) in object coordinate will be projected onto the detector at a point coordinated at (u, v) in detector coordinate (See Fig. 1).

The relationship between two points is represented via the following equation that is a mapping between two coordinates (3D in object coordinate and 2D in detector coordinate)

$$[uw, vw, w]^T = \mathbf{P}[x, y, z, 1]^T, \quad (1)$$

where $\mathbf{P}$ is a 3×4 projection matrix and w is a weighting factor.

The projection matrix $\mathbf{P}$ can be factorized as

$$\mathbf{P} = \mathbf{K}[\mathbf{R} \mid \mathbf{t}], \quad (2)$$

where $\mathbf{K}$ is an (3×3) intrinsic matrix, $\mathbf{R}$ is a (3×3) rotation matrix and $\mathbf{t}$ is a (3×1) translation vector. $\mathbf{K}$ contains intrinsic geometric information about the imaging system, $\mathbf{R}$ is (an orthogonal) rotation matrix that is represented by three Euler angles $\mathbf{R} = \mathbf{R}_z\mathbf{R}_y\mathbf{R}_x$, where $\mathbf{R}_x, \mathbf{R}_y, \mathbf{R}_z$ is the rotation matrix around *x*-,*y*-,*z*- axis, respectively.

From manufacturer's viewpoint, once the projection matrix $\mathbf{P}$ is calculated, it will be factorized into subsequent matrices $\mathbf{K}$, $\mathbf{R}$, and $\mathbf{t}$ from which actual geometric parameters are derived. The extraction process involves the use of RQ decomposition and other normalizations. (A stable implementation of the method is reported in [4]) The calculated value will be compared with the measured value and adjustment will be made to each parameter. The adjusted values will be later used in reconstruction.

In order to measure $\mathbf{P}$ in (1) for each view, we need several pairs of (u_i, v_i) and (x_i, y_i, z_i) with $i = 1,...,N$. To do so, a calibration phantom is needed. The phantom consists of several markers (steel balls) whose centers correspond to (x_i, y_i, z_i) in Eq. (1). The balls are kept in a cylindrical plastic holder. The phantom is designed and manufactured with high accuracy. To find (u_i, v_i), we project the balls onto detector and find the centroid of ellipses that were projection of balls in the projection data. [4, 12].

To accurately find centroid of ellipses, the following steps are used: (i) remove the noise in the projection images using noise filter; (ii) detect edge using Canny edge detector; (iii) locate ellipse center using a curve fitting algorithm which process the detected edge pixels of the ball to result in centroid.

Given the calibration dataset, in this case it is a group of 3D points (x_i, y_i, z_i) where $i = 1,...,N$ (with N is the number of balls in the projection view) and their 2D projected points (u_i, v_i), we can determine the geometric parameters by solving the linear systems of equations (1) via SVD technique or least square optimization technique such as Levenberg-Marquardt algorithm [13]. (More information can be found in [4]).

The projection matrix-based calibration method described above is designed to find geometric parameters for each view of standard CBCT system where all information about phantom is captured in a single view. However, to apply it to offset flat-panel CBCT, some difficulties need to be resolved.

B. Geometric Calibration for Offset Flat-panel CBCT

In offset flat-panel CBCT system, the source-detector axis is often positioned offset to the center of rotation so that the field-of-view of a scanner can be enlarged. This extension posts difficulties to reconstruction [14, 15] and to geometric calibration. In particular, for a given calibration phantom, in each view, projection image contains the projection information about only a portion of the object.

In this work, we design a phantom which has structure as illustrated in Fig. 2. The phantom was made by 24 metal balls, each is a sphere with diameter of 2 mm. These 24 balls are distributed into two circular shapes with the diameter of 110 mm. The distance between two virtual circles is 25 mm. If the phantom is positioned so that its center is approximately matched with the center of rotation of the CT scanner, all projection views contains almost the same structural information about the phantom.

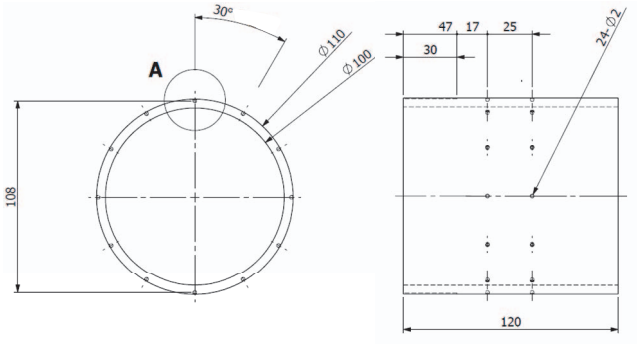

(a) (b)

Fig. 2. Design of the calibration phantom for offset-flat panel CBCT.

To estimate projection matrix for a projection view, we need to have two lists sorted in the same order: coordinates of center of steel balls in the object coordinate (x_i, y_i, z_i) with $i = 1, ..., N$, and coordinates of its projection in the projection (detector) coordinate (u_i, v_i) with $i = 1, ..., N$. (For offset flat-panel CBCT system, the number of visible balls in the projection image is less than N, and in our configuration it varies between 14 and 16). While we have the full first list of object coordinate, the associated one in projection coordinate is difficult to construct since only few balls are visible for a particular projection view. Therefore, it is difficult to (label or) match the center of ball in object coordinate with its corresponding projected center in projection image. (See Fig. 3 for illustration).

Fig. 4 illustrates our method to label balls in projection image. First, we separate the projection balls into two groups, upper and lower ones. Then we find the centers of all ellipses using the ellipse fitting technique. From the calculated centers of ellipses (a.k.a ball centers), we calculate the virtual center of these ball centers. The angles between each ball center and horizontal axis crossing the virtual center will be measured. The balls are then ordered and labeled according to the measured angles. The resulting list is perfectly matched with the one in object coordinate.

C. Geometric Parameters in Reconstruction Algorithms

The geometric parameters define the system matrix which is used in all reconstruction methods, from well-known Feldkamp Davis Kress's algorithm to advanced statistical reconstruction methods. In particular, geometric parameters are used to construct the forward (system) projection matrix which is the key in performing projection and backprojection operations. As an example, we consider the relaxed ordered-subset convex (OSC) algorithm [16] which is a widely used algorithm in the field due to its advantage in providing high quality reconstruction with lower radiation dose.

The update equation of OSC algorithm can be written as follows:

$$\mu_j^{(n,m+1)} = \mu_j^{(n,m)} + \lambda \mu_j^{(n,m)} \frac{\sum_{i \in S(m)} a_{ij} (\bar{p}_i - p_i)}{\sum_{i \in S(m)} a_{ij} \bar{p}_i g_i}, \quad \forall j \qquad (3)$$

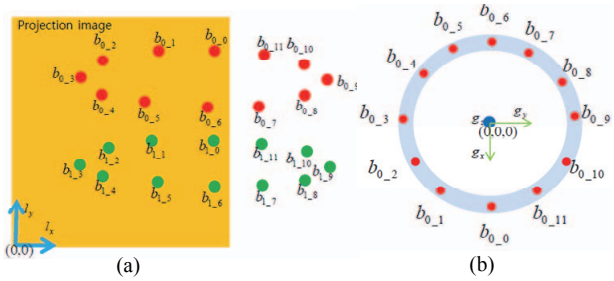

(a) (b)

Fig. 3. Illustration of phantom projection and labels of balls (centers) in the projection image. (a) a representative projection image where only part of phantom is imaged; (b) axial view.

Fig. 4. Method to label balls in projection image. For each group, the virtual center is first calculated, then the angle of each ball with the horizontal axis crossing virtual center will be calculated and used to determine its label. The cross sign indicates the centroid calculated using ellipse fitting technique.

where $g_i = \sum_j a_{ij} \mu_j^{(n,m)}$, $\bar{p}_i = b_i \exp(-g_i)$, μ is the attenuation coefficient map (the image) to be reconstructed, a_{ij} denotes the element of the forward projection matrix which weights the contribution of the voxel indexed by j to the detector bin indexed by i, $\bar{p}_i$ is the expected number of transmission counts in detector element i, n is the iteration number, m is the subset number, λ is the relaxation parameter, p_i is the measured number of transmission counts in detector element i, b_i denotes the blank scan counts in the i-th bin, and $S(m)$ contains the projection in subset m. a_{ij} is usually modeled by the intersecting chord length of the voxel j with the the ray which is defined by the line connecting the source and the center of detector bin i [17]. To measure a_{ij}, we need to know the two end points of the line i. These two end points are indicated by the geometric parameters measured in Section II.A.

In particular, once the projection matrix **P** is computed, we also get the intrinsic matrix **K**, rotation matrix **R**, and translation vector **t**. From **R** and **t**, the source position is given by $\mathbf{c} = -\mathbf{R}^T \mathbf{t}$. That is one end point of the line i. The other end point of the ray i is located at (x, y, z) and calculated as follows

$$[\omega x, \omega y, \omega z, \omega]^T = \mathbf{P}^{\dagger}[u, v, 1]^T \quad (4)$$

where (u, v) is the coordinate of center of detector bin i in detector space, ω is a distance weighting factor, and $\mathbf{P}^{\dagger}$ is a 4×3 pseudo (right) inverse of $\mathbf{P}$ which is given by $\mathbf{P}^{\dagger} = \mathbf{P}^T(\mathbf{P}\mathbf{P}^T)^{-1}$.

It is important to note that in the conventional methods (which are widely used in practice), after estimating **P**, the actual geometric parameters embedded in **R**, **K**, **t** are derived via decomposition techniques. These decomposition techniques require some assumptions about the system such as the upper triangular intrinsic matrix **K** and rectangular pixels in the detector. Therefore, the degradations due to the decomposition techniques are unpreventable. Furthermore, the geometric parameters are then corrected to make it close to actual values provided by the manufacturer when setting up the system. Unfortunately, the new projection matrix generated by the corrected geometric parameters is different from the initially estimated one. That leads to errors in projection and backprojection. In our proposed method, by directly using **P** and its pseudo inverse $\mathbf{P}^{\dagger}$ for backprojection and projection, we can completely eliminate the above error. (Though numerically the decomposed geometric parameters might lightly differ from the ones measured physically).

III. Results

To evaluate the performance of the proposed method, we performed the experiment with a real scanner. The offset flat-panel CBCT system used in this work was a Papaya 3D™ scanner from Genoray Co., Ltd, South Korea. The detector of scanner had the size of $128.6mm\times130.5mm$. The detector bin size was of $(01.mm\times0.1mm)$ which makes the detector having resolution of 1286×1305. Other parameters were determined from calibration process. The calibration phantom was manually made. A software version of calibration phantom was also generated for evaluating purpose.

The calibration phantom was illuminated using real CBCT scanner to generate projection data. The new method was applied to the acquired projection data to estimate the geometric parameters. The estimated geometric parameters were then used to perform projection in software simulator with the software version of the calibration phantom (using the ray-tracing method with the value of blank scan set to $b = 4095$) - followed by a comparison between actually acquired projection image and the software-generated projection image. Finally, the estimated values of geometric parameters were then also used to reconstruct image from several projection datasets.

Fig. 5 shows the a projection image of calibration phantom acquired from the scanner and the one generated from software simulator with the geometric parameters estimated from the acquired projection image. Note that while the acquired projection image was contaminated by Poisson noise in acquisition process, the simulated one was noiseless image. Though two images were different in intensity values, the shapes were exact matched (as shown in the superposed edges in Fig. 5(a)).

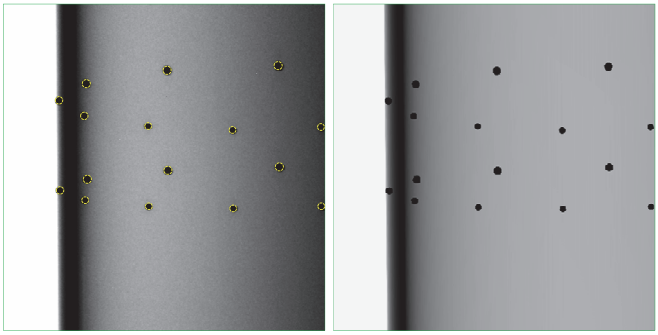

(a) (b)

Fig. 5. (a) Projection image acquired from scanner using the real calibration phantom; (b) projection image generated from software simulator using software phantom and estimated geometric parameters from (a). The superposed edges in (a) are the edges from (b) which show identically shape between two projection images.

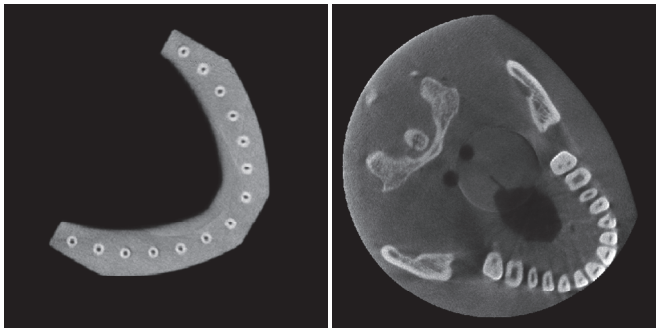

(a) (b)

Fig. 6. OSC reconstructions from real data: (a) arch phantom; (b) skull phantom. The blur rings in the center of two images are due to central artefacts in the offset CBCT system, not geometric parameters.

Using the geometric parameters estimated above, we performed the reconstruction with two datasets: one for arch phantom and the other for skull phantom (those two phantoms are in a laboratory at Genoray Co., Ltd.). The OSC algorithm was used to reconstruct image. The reconstructed images in Fig. 6 clearly show the inner structure of object with sharp edges. Note that in Fig. 6, the blur rings in the center of two images are due to central artefacts in the offset CBCT system and have nothing to do with geometric parameters. We can reduce it by using additional weight factor as in [14, 18]. However, we did not use it since we want to clearly show the contribution of geometric parameters to reconstructions.

IV. Conclusions

We have developed a calibration method for offset flat-panel CBCT system which can accurately determine the geometric parameters for each projection view. The new method comes with a calibration phantom specially designed to offset flat-panel scanner. We have also introduced the use of pseudo inverse of projection matrix for projection, and projection matrix for backprojection. By using projection matrix and its pseudo inverse (not decomposing the projection matrix into subsequent elements as in previous works), we prevent the numerical errors hidden inside the intrinsic matrix

(and other factors) that might cause degradation in projection, backprojection, and thereby the reconstruction. The proposed method was tested with real data experiment where it provides accurate result and satisfactory reconstruction.

Though one can argue that the projection matrix-based geometric calibration relies on dedicated phantom to achieve precise results, the projection matrix used in this work has been illustrated to work well with offset flat-panel CBCT system without the use of very accurate calibration phantom. The new method improves the quality of reconstruction and frees CT makers from time consuming calibration work.

REFERENCES

[1] J. Hsieh, *Computed Tomography: Principles, Design, Artifacts, and Recent Advances*, Second Edition, SPIE Press, 2009.

[2] J. F. Barrett and N. Keat, "Artifacts in CT: Recognition and avoidance," *Radiographics*, vol. 24, no. 6, pp. 1679–1691, 2004.

[3] Y. Cho, D. J. Moseley, J. H. Siewerdsen, and D. A. Jaffray, "Accurate technique for complete geometric calibration of cone-beam computed tomography systems," *Med. Phys.*, vol. 32, no. 4, pp. 968–983, Mar. 2005.

[4] X. Li, D. Zhang, and B. Liu, "A generic geometric calibration method for tomographic imaging systems with flat-panel detectors—A detailed implementation guide," *Med. Phys.*, vol. 37, no. 7, pp. 3844-3854, 2010

[5] A. Ladikos and W. Wein, "Geometric calibration using bundle adjustment for cone-beam computed tomography devices," *Proc. SPIE Medical Imaging*, pp. 83132T, 2012.

[6] D. Panetta, N. Belcari, A. Del Guerra, and S. Moehrs, "An optimization-based method for geometrical calibration in cone-beam CT without dedicated phantoms," *Phys. Med. Biol.*, vol. 53, no. 14, pp. 3841–3861, Jul. 2008.

[7] I. Tekaya, V. Kaftandjian, F. Buyens, S. Sevestre, and S. Legoupil, " Registration-based geometric calibration of industrial X-ray tomography system ", *IEEE Trans. Nucl. Sci.*, vol. 60, no. 5, 2013.

[8] J. Muders, *Geometrical Calibration and Filter Optimization for Cone-Beam Computed Tomography*, PhD Dissertation, Heidelberg University, 2015.

[9] Y. Meng, H. Gong, and X. Yang, "On-line geometric calibration of cone-beam computed tomography for arbitrary imaging objects," *IEEE Trans. Med. Imag.*, vol. 32, no. 2, pp. 278–288, Feb. 2013.

[10] Y. Kyriakou, R. M. Lapp, L. Hillebrand, D. Ertel, and W. A. Kalender, "Simultaneous misalignment correction for approximate circular cone-beam computed tomography," *Phys. Med. Biol.*, vol. 53, no. 22, pp. 6267–6289, Nov. 2008.

[11] J. Wicklein, H. Kunze, W. A. Kalender, and Y. Kyriakou, "Image features for misalignment correction in medical flat-detector CT," *Med. Phys.*, vol. 39, no. 8, pp. 4918–31, Aug. 2012.

[12] R. Hartley and A. Zisserman, *Multiple View Geometry in Computer Vision*, 2nd Ed, Cambridge University Press, 2004.

[13] J. Nocedal and S. Wright, *Numerical Optimization,* Springer, 2006.

[14] E. Hansis, J. Bredno, D. Sowards-Emmerd, and L. Shao, "Iterative reconstruction for circular cone-beam CT with an offset flat-panel detector," in *Proc. IEEE NSS-MIC*, 2010, pp. 2228–2231.

[15] G. Wang, "X-ray micro-CT with a displaced detector array," *Med. Phys.*, vol. 29, pp. 1634–1636, 2002.

[16] J.S. Kole and F.J. Beekman, "Evaluation of the ordered subset convex algorithm for cone-beam CT," *Phys. Med. Biol.*, vol. 50, pp. 613-623, 2005.

[17] R. L. Siddon, "Fast calculation of the exact radiological path for a threedimensional CT array," *Med. Phys.*, vol. 12, no. 2, pp. 252–255, 1985.

[18] V.-G. Nguyen and S.-J. Lee, "Parallelizing a Matched Pair of Ray-Tracing Projector and Backprojector for Iterative Cone-Beam CT Reconstruction," *IEEE Trans. Nucl. Sci.*, vol. 62, no. 1, pp. 171-181, 2015.